

Artificial Symmetry-Breaking for Morphogenetic Engineering Bacterial Colonies

Isaac N. Nuñez,^{#,†,⊥} Tamara F. Matute,^{#,†,⊥} Ilenne D. Del Valle,^{#,‡} Anton Kan,[§] Atri Choksi,^{||} Drew Endy,^{||} Jim Haseloff,[§] Timothy J. Rudge,[†] and Fernan Federici^{*,‡,§,⊥}

[†]Escuela de Ingeniería, Pontificia Universidad Católica de Chile, 7820436, Santiago, Chile

[‡]Departamento de Genética Molecular y Microbiología, Facultad de Ciencias Biológicas, Pontificia Universidad Católica de Chile, 8331150, Santiago, Chile

[§]Department of Plant Sciences, University of Cambridge, Downing Street, Cambridge, CB2 3EA, United Kingdom

^{||}Department of Bioengineering, Stanford University, Stanford, California 94305, United States,

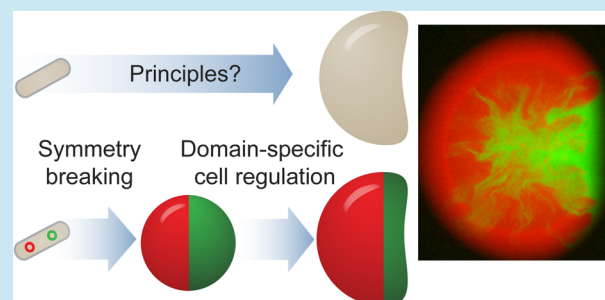
[⊥]Fondo de Desarrollo de Areas Prioritarias Center for Genome Regulation, Millennium Nucleus Center for Plant Systems and Synthetic Biology, Pontificia Universidad Católica de Chile, 7820436, Santiago, Chile

Supporting Information

ABSTRACT: Morphogenetic engineering is an emerging field that explores the design and implementation of self-organized patterns, morphologies, and architectures in systems composed of multiple agents such as cells and swarm robots. Synthetic biology, on the other hand, aims to develop tools and formalisms that increase reproducibility, tractability, and efficiency in the engineering of biological systems. We seek to apply synthetic biology approaches to the engineering of morphologies in multicellular systems. Here, we describe the engineering of two mechanisms, symmetry-breaking and domain-specific cell regulation, as elementary functions for the prototyping of morphogenetic instructions in bacterial colonies.

The former represents an artificial patterning mechanism based on plasmid segregation while the latter plays the role of artificial cell differentiation by spatial colocalization of ubiquitous and segregated components. This separation of patterning from actuation facilitates the design-build-test-improve engineering cycle. We created computational modules for CellModeller representing these basic functions and used it to guide the design process and explore the design space *in silico*. We applied these tools to encode spatially structured functions such as metabolic complementation, RNAPT7 gene expression, and CRISPRi/Cas9 regulation. Finally, as a proof of concept, we used CRISPRi/Cas technology to regulate cell growth by controlling methionine synthesis. These mechanisms start from single cells enabling the study of morphogenetic principles and the engineering of novel population scale structures from the bottom up.

KEYWORDS: morphogenetic engineering, synthetic biology, morphogenesis, CRISPR, modeling



Synthetic biology is changing our perception of biological systems as a mere source of raw material to a vision of biology as a programmable substrate for material fabrication, chemical production, and computing.^{1–11} The use of design specifications, computer-assisted mathematical modeling, and novel DNA fabrication methods have made possible the engineering of biological functions and systems of increasing reliability, scale and complexity.^{7,8,12–18} However, the scalability of circuit size within single cells has been limited by metabolic burden effects, cross-talk interactions, and genetic instability, a limitation reflected in the number of engineered components per cell.¹⁹ Engineering at the multicellular scale has emerged as a solution to the limitations encountered at the single cell level. The engineering of multicellular functions has been successfully used to engineer artificial consortia, patterning, and distributed computing in microbial systems.^{6,20–27} Defining elementary functions for morphogenetic engineering could complement

these developments by providing mechanisms for the establishment and maintenance of higher order structures. Morphogenetic engineering, is an emergent field founded by Doursat et al.^{28,29} that explores the artificial design of autonomous systems capable of developing complex morphologies. Its emphasis is on the programmability and controllability of self-organization toward the reproducible emergence of collective architectures. Morphogenetic engineering will be critical for engineering tissues, microbial consortia, and living functional materials.³⁰

Engineering morphogenetic mechanisms in biological systems is a challenge that requires the formulation of new approaches and tools. Morphogenesis involves multiparallel, collective and emergent processes across different spatial and temporal scales,^{31,32} which makes the process intractable from

Received: May 21, 2016

Published: October 30, 2016

the engineering perspective. Engineering practices rely on design specifications and elementary functions that are easy to abstract, simulate and implement with predictable core components. This provides tractability for the design-build-test iterative cycle, making the process more informative and reproducible. Aircraft engineering, for instance, relies on principles of flight: lift, propulsion and control; whereas birds integrate these three elementary functions as a whole in their flapping wings (reviewed in^{33,34}). Although the use of fixed wings and the decoupling of lift, propulsion and control seem unnatural and almost contradictory from the avian flight perspective, it provides the mechanistic abstractions that makes the engineering process more tractable. This approach is in line with the synthetic biology mantra of abstraction, modular design and principle-based engineering that allows implementation from characterized core components that fit into the design specifications of the system. Abstracting the complexity of biological processes into well-defined elementary functions has already facilitated the engineering of multicellular patterns.^{21,23,25,35,36} Computational methods for *in silico* engineering of shapes from fundamental collective phenomena have been developed.³⁸ However, the development of tools and resources for prototyping morphogenetic mechanisms remains less explored.^{29,39,40}

Here, we describe the development of computational models and genetic tools for prototyping morphogenetic mechanisms in bacterial colonies. With the aim of gaining tractability, debugging capabilities, and scalability in the process, we have defined two elementary functions: symmetry-breaking and domain-specific cell regulation. These are inspired by two natural process: (i) symmetry-breaking in developing embryos and (ii) domain-specific organogenesis during flower development, a process guided by the colocalization of transcriptional regulators.⁴¹ We implemented these two functions as a system of ubiquitous and segregating plasmids that facilitates modular and combinatorial prototyping of instructions. We also defined these elementary functions as explicit computational modules in CellModeller,^{42,43} which helped to define important properties of the system. CellModeller is an individual-based biofilm modeling platform that computes the growth of colonies of rod-shaped bacteria from a single initial cell. It uses a growing rigid-body method to compute the non-overlapping positions and orientations of elongating cells subject to minimizing work done in overcoming viscous drag. This leads to dominant growth at the colony margin. It also allows simulation of internal cell states such as plasmid content and effects of plasmid gene expression. We applied these methods and resources to the programming of bacterial colony shapes using CRISPRi/Cas9 regulation of cell growth.

RESULTS AND DISCUSSION

Overview of the Platform: A Two-Step Mechanism for Morphogenetic Programming. The goal of this work was to develop a simple system for prototyping morphogenetic engineering mechanisms. This system would allow starting from a single cell and controlling shape at the multicellular level using growing bacterial colonies as simple systems (Figure 1A). With the aim of having more tractability during the design-build-test process, we defined two abstract elementary functions: (i) symmetry-breaking and (ii) domain-specific cell regulation (Figure 1B). The first step was intended to establish polarity and domains of cells in the colony; while the second was intended to regulate cells differentially within these

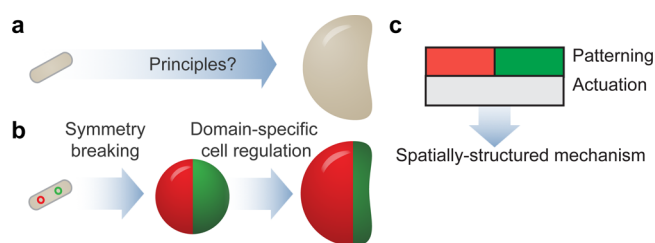


Figure 1. Abstract elementary functions for morphogenetic programming. (a) Schematic representation of a morphogenetic engineering challenge. (b) Adoption of two elementary functions to address this task: symmetry-breaking and domain-specific cell regulation. (c) Schematic representation of the two-tier organization of genetic layers that implement these elementary functions.

domains (Figure 1B). To implement these two steps, we sketched a two-tier organization model inspired by the ABC model of flower development that exploits the spatial coexistence of transcriptional regulators to instruct organogenesis⁴¹ (Figure 1C). This design would allow the implementation of instructions by interchanging plasmid combinations.

Patterning Layer: Symmetry Breaking Function for the Establishment of up to Four Different Domains Per Colony. Symmetry-breaking phenomena, as the process of reducing homogeneity to generate more structured systems,⁴⁴ have been intensively studied in chemical, physical, and biological systems.^{32,45–50} From an engineering point of view, symmetry breaking is key in establishing the first coordinates within an otherwise homogeneous system from where higher order structures and dynamics can be built in search for increasing functional specialization at different scales.

We implemented a symmetry-breaking step, the first elementary function, as a system of segregating plasmids (Figure 2A). This mechanism is based on an artificial tool created to label multiple cell lineages in growing bacterial colonies.⁴³ These plasmids create domains of cells in colonies by segregating from a single cell acting as a colony founder (Figure 2B). This process relies on the segregation of two plasmid variants containing different antibiotic resistance genes (e.g., A1 or A2), spectrally distinct fluorescent proteins but a common plasmid backbone with a third antibiotic resistance gene (e.g., A3) (Figure 2B). When cotransformed and grown in the presence of antibiotics A1 and A2, both plasmid variants are maintained in the same cell. When transferred to a growth media containing antibiotic A3 only, cells are unable to distinguish between the two plasmid variants, leading to a stochastic segregation of these two into different daughter cells. This creates cell lineages harboring only one of the two plasmid variants and its corresponding fluorescent protein (Figure 2C). This system relies on the mechanical properties of bacterial colony growth⁴³ to create radial domains of cells as colonies grow from a single cell. From a morphogenetic engineering perspective, we were interested in the establishment of two to six domains per colony. Colonies composed of two domains only (i.e., bipartite) were of particular interest due to their simplicity and resemblance to the process of polarity establishment in developing embryos.⁵⁰

We created biophysical models of these processes to guide the engineering of these patterned colonies (Figure 2C) (see Supporting Information Movie S1, S2, and S3). We designed a CellModeller plasmid segregation module to explore the effects of copy number on the formation of sectors within colonies.

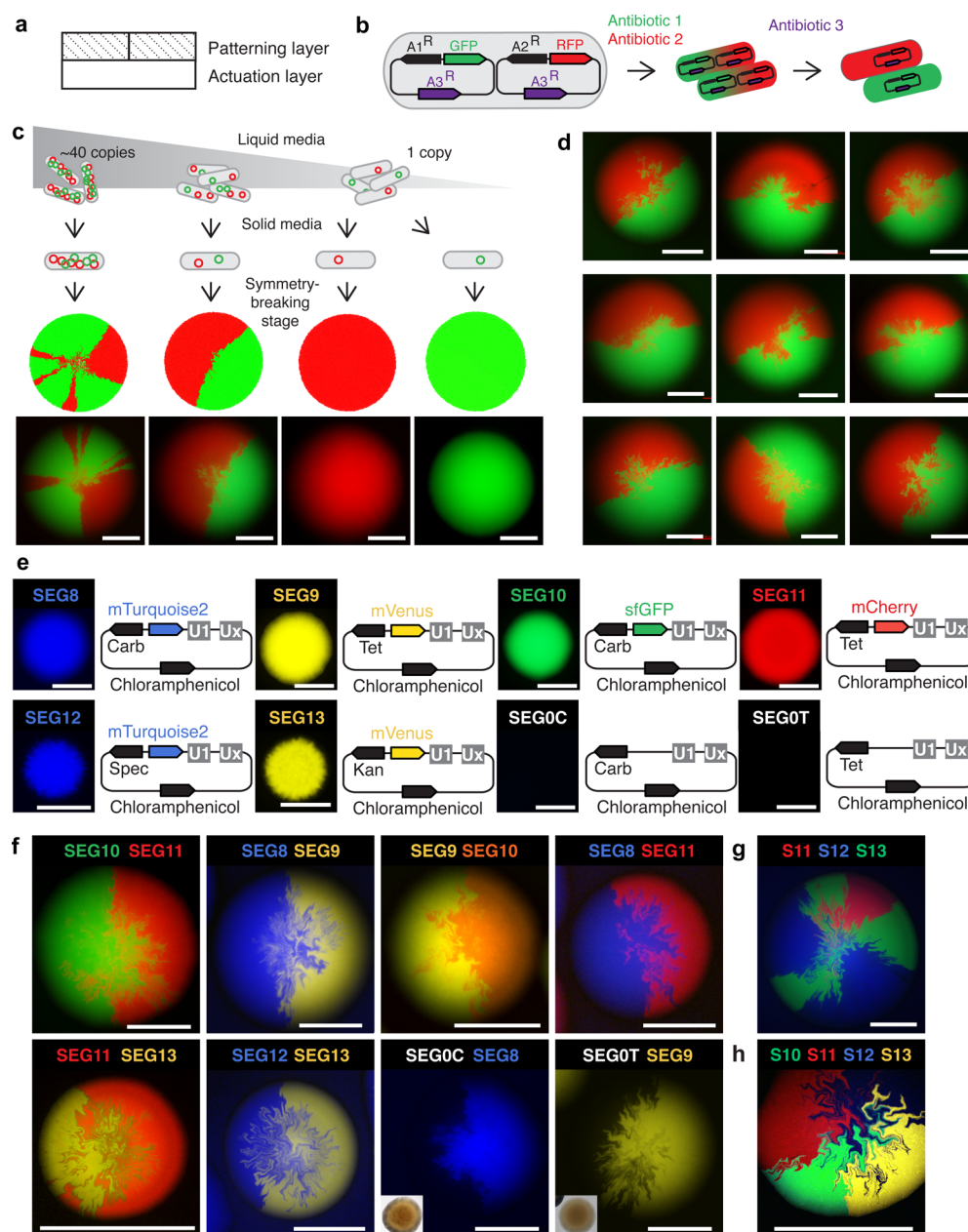


Figure 2. Genetic implementation of the patterning layer. (a) Schematic representation of the two-tier plasmid organization highlighting the patterning layer. (b) Schematic representation of the antibiotic-based regulation of plasmid maintenance within cells. Growing cells in the presence of A1 and A2 antibiotics maintains the two plasmid variants (red and green) within cells. These variants segregate in the presence of antibiotic A3 cells due to the presence of an antibiotic resistance gene located in the backbone that is common to both plasmid variants. Thus, cells maintain plasmids without any preferences for the two variants (either red or green) giving rise to cells containing one or the other (shown as red and green cells). (c) Schematic representation of copy number effect on the formation of bipartite and multisector colonies. The protocol starts with cells growing in liquid media containing arabinose, the high copy number inducer. Plating cells (i.e. colony forming units) at different points after removing arabinose from liquid culture permits starting colonies with different amounts of the two plasmid variants. Plating at later stages, when cells are close to maintain only two copies/cell of the plasmid, increases the likelihood of creating bipartite colonies as shown by CellModeller simulations and experimental data (bottom). (d) Representative bipartite colonies obtained with this protocol. (e) Epifluorescence image of colonies bearing different variants of SEG plasmids: SEG8 (blue), SEG9 (yellow), SEG10 (green), SEG11 (red), SEG12 (blue), SEG13 (yellow), and SEG0C/SEG0T, which do not carry a fluorescent marker in their backbone. (e–g) Colonies showing the segregation of different combinations of two (f), three (g), and four (h) SEG plasmids. Scale bar, 500 μm .

Biophysical parameters of growth were chosen based on a previous work to reproduce the growth of colonies in high resolution confocal microscopy. Growth was restricted to 2-dimensions for simplicity. Simulations were initiated with a single cell containing equal numbers (N) of each of two types of plasmid ($2N$ plasmids in total). On cell division each plasmid

replicated and each daughter cell inherited $2N$ randomly selected plasmids with equal probability of each type. Simulations starting with cells containing 10 (see Supporting Information Figure S1A) and 4 copies (see Supporting Information Figure S1B) only produced colonies with multiple domains. To test this further, we engineered segregation

plasmids bearing the low copy origin of replication pSC101*,¹⁶ considered to maintain 4–10 copies per cell. As suggested by simulations, these plasmids created colonies of multiple domains and failed to show the formation of bipartite colonies (see Supporting Information Figure S1C).

According to our model, we needed to reduce the copy number to an ideal state of 2 copies per cell (one copy of each of the two plasmid variants) in order to favor the formation of bipartite colonies with a possibility of 33% (see Supporting Information Figure S1D–F). We used a backbone from the pDestBAC plasmid,⁵¹ whose copy number can be controlled with arabinose from 1 to ~40 (see Supporting Information Figure S2A–C). This system allowed us to maintain the two plasmids in the same cell at medium copy while grown in liquid culture supplemented with A1, A2, and arabinose (i.e. “plasmid propagation stage”) and decrease to single copy when transferred to liquid culture without the arabinose (i.e. “plasmid copy decay stage”) (Figure 2C). Thus, we could grow single cells as colony-forming units in solid media at the point when they contained 2 copies per cell, favoring the formation of bipartite colonies (i.e., “symmetry-breaking stage”).

We used tetracycline and ampicillin resistance cassettes for A1–A2 coselection during the plasmid propagation stage; and a chloramphenicol resistance marker in the backbone as the common antibiotic resistance for the plasmid copy decay stage and the symmetry-breaking stage (Figure 2C, see Supporting Information Figure S2A). We developed a protocol to increase the probability of generating bipartite colonies by changing the length of time that cells were maintained in the plasmid decay stage before being plated onto solid media for symmetry-breaking (Figure 2C). Two independent experiments indicated that 180 min of growth at the plasmid decay stage produced the maximum ratio of bipartite colonies (see Supporting Information Figure S2D–E). Following this protocol, we were able to create bipartite colonies reliably (Figure 2C, see Supporting Information Figure S2F), demonstrating the implementation of the symmetry-breaking elementary function. Unexpectedly, we also observed bipartite colonies at earlier stages when cells were supposed to be in high copy state (see Supporting Information Figure S2F). This could be due to the variability on copy number per cell and unbalanced proportion of plasmid variants in cells grown in liquid cultures. This will inevitably cause a wider distribution of states at the moment of plating cells on solid media.

Being able to program a single cell (colony founder) to trigger morphogenetic changes taking place at the colony level was essential for our aim of prototyping morphologies from the bottom up. It was therefore essential to avoid false bipartite colonies, products of colonies “crashing” into each other during growth in close proximity. For this, we performed controls to identify cell dilutions that increase the chances of getting those unwanted colonies. We found that having a density above 7 colonies/cm² always produced false colonies. We therefore work with densities below 1–3 colonies/cm², which we control by diluting cells accordingly before plating (see Supporting Information Figure S3).

Next, we created a series of SEG# plasmids carrying different fluorescent protein genes in their backbone (sfGFP, mTurquoise2, mVenus, and mCherry) and no fluorescent markers (Figure 2D). The use of four different antibiotic resistance cassettes (kanamycin, spectinomycin, tetracycline, and ampicillin) allowed us to segregate different combinations of two, three, and up to four plasmids (Figure 2E–G). These plasmids

showed no significant effect on cell growth (see Supporting Information Figure S4). These vectors were also engineered to contain unique nucleotide sequences “UNS”⁴⁹ that facilitate combinatorial assembly of instructions from a library of transcriptional units. We created a library of UNS-flanked transcriptional units containing terminators from a list of synthetic strong terminators⁵² (see Supporting Information Figure S5). These results demonstrate that we could use this system to control symmetry-breaking of growing bacterial colonies and establish up to four different cellular states reliably.

Actuation Layer: An Ubiquitously Distributed Plasmid to Encode Domain-Responsive Functions. Following the organizational strategies describe in Figure 1, we created vectors of ubiquitous localization across the colony (Figure 3).

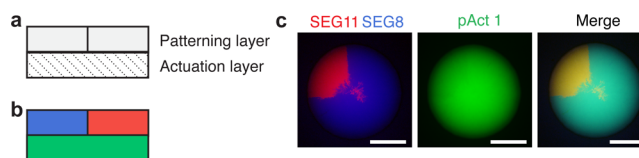


Figure 3. Genetic implementation of the actuation layer. (a) Schematic representation of the two-tier plasmid organization highlighting the actuation layer. (b) Schematic representation of the genetic implementation by the colocalization of the patterning layer composed of SEG vectors (in blue and red), and actuator layer composed of pAct ubiquitous vector (in green). (c) Genetic implementation of this organization by SEG plasmids SEG8 and SEG11, and actuation plasmid pAct1 expressing mVenus (in green). A merged image is shown to highlight the colocalization of plasmids. Scale bar, 500 μm .

These pAct vectors contained actuator genes that regulate different cellular processes in response to or in combination with other regulators being expressed from the patterning layer (SEG plasmids). This process corresponds to the second step in our approach, the domain-specific regulation of cellular processes (Figure 1B). pAct# vectors were designed as low copy plasmids (pSC101*,¹⁶) containing UNS sites to facilitate the combinatorial assembly of transcriptional units. To demonstrate the ubiquitous and sectorized localization of genes from pAct and SEG plasmids, respectively, we expressed mVenus from pAct1, mTurquoise2 from SEG8, and mCherry from SEG11 (Figure 3B,C). These results show how this two-tier organization can be used to superimpose spatial rules over ubiquitous functions.

Domain-Specific Regulation of Colonies: Metabolic Complementation, RNAP7 Activation and CRISPR-Regulation of Gene Expression. To validate the utility of this two-tier organization, we used it to control a series of different cellular functions within the created domains. The concept of domains, along with the maintenance of their boundaries, has been central to the understanding of biological morphogenesis (see a review, ref 53). We propose the use of these domains to assign artificial states and functions to a different part of the colony. First, we applied it to the domain-specific complementation of an incomplete metabolic pathway. We used the five-enzyme metabolic pathway from *Chromobacterium violaceum* controlling the production of violacein.⁵⁴ A synthetic operon containing the five enzymes VioA, VioB, VioC, VioD, and VioE, was used in these experiments (Figure 4A). We constructed pAct2 carrying genes vioA, B, and E that catalyze the conversion of tryptophan to prodeoxyviolacein, which spontaneously become deoxychromoviridans, a green-

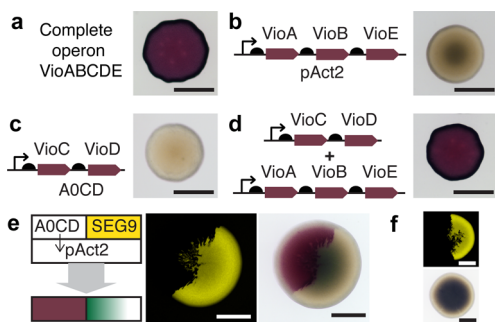


Figure 4. Domain-specific metabolic pathway complementation. (a) Colony showing violacein production from complete VioABCDE violacein operon. (b) Colony expressing *vioC* and *vioD* genes from vector A0CD. (c) Colony showing deoxychromoviridans production from vector pAct2 containing genes *vioA*, *vioB*, and *vioE*. (d) Colony showing violacein production from the cotransformation of vectors A0CD and pAct2. (e) Domain-specific metabolic complementation of violacein synthesis pathway. SEG9 was used as a segregation partner of A0CD. (f) Segregating control SEG9 and SEG0C on top of pAct2 showed no violacein synthesis. Scale bar, 500 μm .

colored compound⁵¹ (Figure 4B). This plasmid was expressed ubiquitously across the colony producing a faint green color in cells located in the center of the colony (Figure 4B). Next, we constructed the segregating plasmid A0CD carrying the genes *vioC* and *vioD*, which was unable to produce any visible pigment on its own (Figure 4C) but produced a purple pigment in combination with *vioABE* due to the conversion of prodeoxyviolacein to violacein (Figure 4D). When segregated with SEG9 on top of ubiquitously located pAct2, A0CD produced violacein in a domain-specific manner as expected from the complementation of ABE pathway with CD genes (Figure 4E). No violacein synthesis was observed when SEG9 and pAct2 were combined with control SEG0C (Figure 4F), a colorless segregating plasmid (Figure 4D).

Next, we explored the segregation of transcriptional controllers acting on target genes located on pAct vectors. We created S8T7 segregation plasmid, carrying the RNA polymerase from phage T7, and pAct3, carrying *mCherry* gene downstream of T7 promoter. The T7 RNAP was expressed from a pLac promoter in order to regulate its expression with a *lacI* repressor constitutively expressed from pAct3. We used IPTG to regulate the expression of *mCherry* from pAct3 in the presence of S8T7 (see Supporting Information Figure S6A). The segregation of S8T7 and SEG9 plasmids on top of pAct3, located ubiquitously across the colony, showed domain-specific activation of *mCherry* upon IPTG induction (Figure 5A). Conversely, control experiment segregating SEG9 and SEG8

failed to induce *mCherry* from pAct3 (see Supporting Information Figure S6B). Next, we used split T7 RNAP⁵⁵ to reduce background expression in the absence of IPTG. We created a segregating plasmid S8BST7 and ubiquitous plasmid pAct4 carrying the $\beta\sigma$ and α fragment of T7 RNAP, respectively (Figure 5B). The segregation of S8BST7 with SEG11 led to domain-specific spatial regulation while IPTG provided temporal control of *mVenus* expression (Figure 5B). This system was shown to activate two target genes simultaneously (see Supporting Information Figure S6C).

To further explore the utility of our system, we performed CRISPRi/Cas9 regulation of gene expression in a domain-specific manner. We targeted VioABCDE synthetic operon to repress the production of the visible pigment violacein. First, we made constructs to test different sgRNAs targeting *VioA* and *VioC* genes (see Supporting Information Figure S7), and selected sgRNA-*VioC*. Next, we created the segregation vector SVioC containing constitutively expressed sgRNA-*VioC* and *dCas9*. This construct shut down violacein production in a domain-specific manner when segregated with SEG0C on top of the ubiquitously expressed VioABCDE operon (Figure 6A). All these experiments together demonstrated the versatility of our system for the spatial and temporal regulation of cellular functions in bacterial colonies.

Prototyping Morphogenetic Instructions by Symmetry-Breaking and Domain-Specific Cell Growth Regulation. We applied this toolkit to the creation of a tractable morphogenetic mechanism in bacterial colonies. We used CRISPRi/Cas9 regulation of *MetA* gene expression as a mechanism to regulate colony growth via induced methionine auxotrophic cells. First, we designed a series of vectors containing a *LacI*-regulated *dCas9* and the constitutive expression of one of four sgRNAs (*sgMet-a*, *-b*, *-c*, *-d*) targeting the *metA* gene in the genome. These plasmids also included a 5' fusion of the first 156 nt of *MetA* to *sGFP* as a fluorescent reporter of *MetA* expression inhibition (see Supporting Information Figure S8A). After comparing the inhibition strength of the four sgRNAs (see Supporting Information Figure S8B), *sgMet-a* was selected for CRISPRi-induced cell growth regulation (see Supporting Information Figure S8C and D). We added methionine to demonstrate that the effects were due to *MetA* regulation and not by *dCas9* expression (see Supporting Information Figure S8D). Following the two-tier approach, we created S11Ma and S8Ma vectors to segregate *sgMet-a* as red and blue domains, respectively, and pAct6 to ubiquitously express *dCas9* under IPTG regulation (Figure 7A and B). This system was proven successful in the regulation of cell growth in liquid culture (see Supporting Information

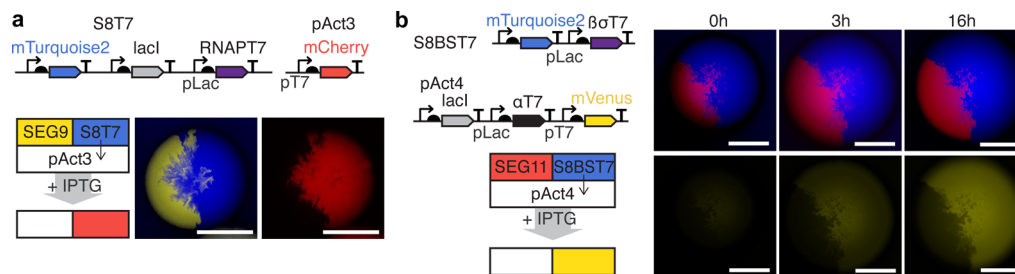


Figure 5. Domain-specific activation of gene expression. (a) Segregation of RNAP T7 from S8T7 (in combination with SEG9) showing the induction of *mCherry* from pAct3 upon IPTG treatment. (b) Temporal and spatial regulation of *mVenus* induction in colonies segregating SEG11 and S8BST7 in combination with pAct4. IPTG induced α and $\beta\sigma$ RNAP T7 fragments from pAct4 and S8BST7, respectively. Scale bar, 500 μm .

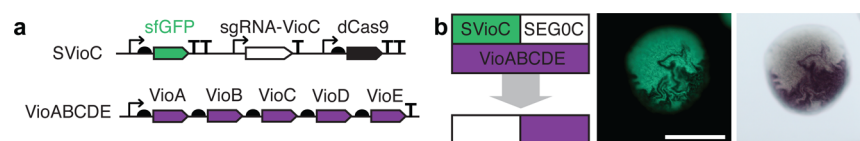


Figure 6. Domain-specific CRISPRi/Cas9 regulation of gene expression. (a) Schematic representation of spatial regulation of violacein production from *VioABCDE* by *SVioC* segregating plasmid. (b) Scale bar, 200 μm .

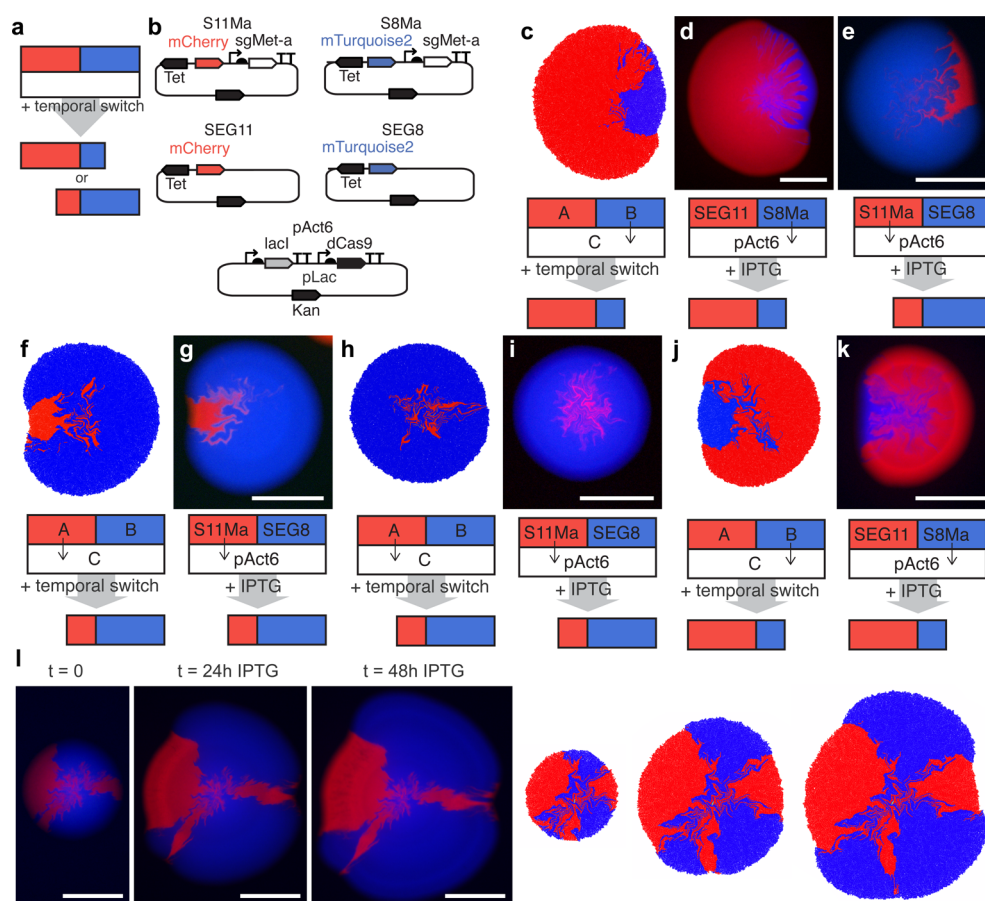


Figure 7. Morphological changes in bacterial colonies induced by symmetry-breaking and domain-specific cell growth regulation. (a) Two tier organization for morphogenetic regulation. (b) Organization of *S11Ma* and *S8Ma* plasmids containing *sgMet-a* and *pAct6* plasmid containing *dCas9* ubiquitously. (c–k) Representative images and simulations capturing the most frequent morphologies from three independent experiments. (l) Time lapse sequence of a representative colony showing the effect of initial patterns on the evolution of the morphology in both data and simulations. Scale bar, 500 μm .

Figure S9), suggesting that it could be used to induce morphological mechanism in colonies grown on solid media. Following the protocol described in previous sections, we segregated *S11Ma/SEG8* or *S8Ma/SEG11* in cells containing *pAct6* (Figure 7A,B), and subsequently treated them with IPTG, IPTG + methionine, or control solution. We found striking morphological features that were not obtained in control treatments (see Supporting Information Figure S10A–E). We found that the initial pattern of domains significantly influenced the final morphologies (see Supporting Information Figure S10F).

To better understand these effects, we created a CellModeller module that simulates domain-dependent cell growth in a modular organization followed from the modular design of elementary functions. We studied the whole process by simulating the same cell growth regulation step starting from different colony patterns such as bipartite (see Supporting Information Movie S4) and multisected (see Supporting

Information Movie S5) colonies. This facilitates the implementation and debugging of new mechanisms without affecting the rest of the components. We used CellModeller to explore *in silico* different parameters such as initial sector pattern (i.e., bipartite or multisected colony) and onset time for cell growth inhibition, such as triggering differential growth rates in different domains at stage 0, 1000, 5000, and 10000 cells of the simulations (see Supporting Information Movie S6 to S13). Growth rates were determined from plasmid copy numbers to range linearly between 1 (all plasmids promote growth) and 0.5 (no plasmids promote growth). We found that our models captured remarkably most of the observed morphologies in our data (Figure 7C–L). We also identified basic structural features that were over-represented in live and digital colonies (see Supporting Information Figure S10G). Together these data demonstrated that our system allows the implementation of morphogenetic instructions that give rise to reproducible features through tractable mechanisms. This system could act

as a platform to compile spatial instructions from elementary functions and features that would act as building blocks of morphogenesis.^{37,56} These could be also used to control concatenated events that can be tuned externally, similarly to the hierarchical strategies of nanofabrication inspired by biomineralization principles.⁵⁷ Ultimately, the process could be completely self-regulated by feedback signals from global emergent states. We aim to introduce cell–cell signaling to implement this global-to-local bidirectional reinforcing and feedback mechanisms with the aim of engineering self-organized morphologies and higher order dynamics.

CONCLUSIONS

Engineering morphogenesis and self-organization is increasingly gaining attention across different fields from biological sciences to robotics.^{28,37–39,58} Programming morphogenesis in biological systems is essential for constructing living functional materials,^{2,30} engineering microbial consortia with distributed functions,²⁷ and implementing distributed computation schemes.^{6,24,26} Although artificial patterning mechanisms have been already developed with remarkable results,^{21,23,25,35,36} the engineering of morphogenetic mechanisms has remained less explored.³⁸

Morphogenetic engineers face the challenge of designing functioning setups in systems with daunting complexity. The use of tractable instructions and structures could facilitate this process. We seek to apply synthetic biology tools and biophysical modeling to identify elementary functions for programming morphogenesis in simple biological systems such as bacterial colonies. Here, we created artificial mechanisms for patterning and cell differentiation that allowed the regulation of cellular states within the limits of well-defined areas of the colony. The two-tier organization to design and characterize controllers and actuators separately along with the use of modular functions abstracted into computational models in CellModeller, will be critical for gaining tractability in the future implementation of high-level designs from low-level specifications. These tools could also be combined with evolutionary computing approaches and directed evolution to explore emergent behavior and phenotype-to-genotype mappings.

Our system could also be used to benchmark models that integrate different temporal and spatial scales, a challenge for multiscale modeling. These tools could be combined with recent developments^{25,36,59} to set morphological instructions from a single cell recapitulating synthetically what developmental programs do in embryos. This will increase tractability in the process of reverse engineering emergent shapes, providing mechanistic understanding of fundamental processes underlying natural morphogenesis and development. Our platform could also be used in microbial ecology studies, for which spatial organization plays a crucial role in population dynamics.^{60–66} In turn, this could inform the implementation of new morphogenetic metaphors based on ecological functions. Starting from single cells offers the possibility of studying and engineering these phenomena from the bottom up as truly self-organized processes.

METHODS

Extended experimental procedures can be found in the Supporting Information Appendix.

DNA construction. All plasmids were constructed by Gibson assembly.⁶⁷ SEG plasmids and vectors containing each

transcriptional unit flanked with UNs were constructed from backbones pDestBAC and pJT170/2/4/6 series from Pam Silver's lab.⁵¹ pAct plasmids were constructed from backbone pSB4K5 from the Registry of Biological Parts (MIT). The VioABCDE synthetic operon was obtained from the 2009 Cambridge iGEM team (<http://2009.igem.org/Team:Cambridge/Project/Violacein>). RNAPT7, promoters and fluorescent proteins were obtained from the Registry of Parts (MIT). dCas9 was obtained from Luciano Marrafini via Addgene. All the sequences and plasmids can be found at Addgene. PCR fragments were amplified using Phusion High-Fidelity DNA Polymerase (NEB) and visualized using SYBR Safe (ThermoFisher) on a blue LED transilluminator (iorodeo.com). Purification of plasmids and PCR fragments was performed using Wizard Plus SV Minipreps DNA Purification System and Wizard SV Gel and PCR Clean-Up System (both of Promega), respectively. Primers were supplied by IDT ([idtdna.com](http://www.idtdna.com)). We used the following primers for combinatorial assemblies of UNS-flanked genes:

U1F: CATTACTCGCATCCATTCTCAGGCTG and U2R: GCTTGGATTCTGCGTTTGTTCGTC for genes flanked between UNS1 and UNS2, U2F: GCTGGGAGTTCGTAGACGGAAACAAC and U3R: CGACCTTGATGTTCCAGTGCGATTG for genes flanked between UNS2 and UNS3, U3F: GCACTGAAGTCCCTCAATCGCAC and U4R: GACTTTGCGTGTGTCTTACTATTGCTGG for genes flanked between UNS3 and UNS4, U4F: CTGACCTCCTGCCAGCAATAGTAAG and UXR: GGTGGAAGGGCTCGGAGTTGTGG for genes flanked between UNS4 and UNS5-UNSX.

SEG vectors for assemblies were amplified with 1XCF: GTCTGTCTGTGACAAATTGC and U1R: GAGACGAGACGAGACAGCCTGAG; and UXF: CCAGGATACATAGATTACCACAACCTCCG and 1XCR: GAGGGCAATTGTGCAGGGTTAAG. pAct vectors for assemblies were amplified with KAGF: TAATTACTaGTCCTTTTCCcgg-GAGaTcTGGGTATCTGTAAATTCTGCTAGACC and U1R: GAGACGAGACGAGACAGCCTGAG; and UXF: CCAGGATACATAGATTACCACAACCTCCG and KAGR: TACCCAgAtCTCccgGAAAAAGGACtaGTAATTATCAT-TGACTAGCCCATCTCAATTG.

Growth condition. All transformations were performed on *E. coli* Top10 (Invitrogen) made competent by the CCMB80 method (http://openwetware.org/wiki/TOP10_chemically_competent_cells). DH5Z1 cells were used for the segregation of three and four plasmids. Cells were grown on LB (10g of tryptone, 5g of yeast extract, and 5 g of NaCl dissolved in deionized water to a final volume of 1 L) or M9-glucose (1 × M9 salts supplemented with 2 mM MgSO₄·7H₂O, 0.1 mM CaCl₂, 0.4% glucose, and 0.2% casamino acids; 5× M9 salts contains 64 g of Na₂HPO₄·7H₂O, 15 g of KH₂PO₄, 2.5 g of NaCl, and 5 g of NH₄Cl dissolved in deionized water to a final volume of 1 L), where 1.5% w/v agar were used for solid culture. For methionine auxotrophy experiments, cells were grown in M9-glucose supplemented with L-leucine (30 mg/L). For methionine and inducer applications, we prepared a 1000× stock solution (12 g/L) of methionine, 0.1 M of IPTG, and 1 M of L-arabinose and filter sterilized them. Antibiotics were prepared as stock solutions of kanamycin (50 μg/μL), carbenicillin (100 μg/μL), tetracycline (10 μg/μL), or chloramphenicol (10 μg/μL).

Fluorescence Quantification Using Fluorometry. Fluorescence and absorbance were measured in a Clariostar plate

reader (BMG LABTECH), with GFP excited at 470–15 nm and measured at 515–20 nm, RFP excited at 570–15 nm, and measured at 620–20 nm, and absorbance measured at 600 nm.

Microscopy and Image Analysis. A Nikon Ni microscope was used for all experiments except for 4-plasmid segregation experiments. The following filter sets were used for the four fluorescent proteins used in this study: mTurquoise2 (excitation at 425–445 nm; dichroic 455 nm, emission 465–495 nm), GFP (excitation at 465–495 nm; dichroic 505 nm, emission 515–555 nm), mVenus (excitation at 490–510 nm; dichroic 515 nm, emission 520–550 nm), mCherry (excitation at 540–580 nm; dichroic 600 nm, emission 605–695 nm).

4-Plasmid segregation images were obtained using an inverted Zeiss LSM 780 multiphoton laser scanning confocal microscope. Images were taken using a 10X air objective. sfGFP was excited at 488 nm (argon ion laser), RFP was excited at 561 (HeNe laser), mTurquoise2 was excited at 458 (argon ion laser), and mVenus was excited at 488 (argon ion laser). Fluorescence was detected using a 32 anode Hybrid-GaAsP and two standard photomultiplier tubes. sfGFP emission was detected between 499 and 580 nm, RFP emission was detected between 599 and 697 nm, mTurquoise2 emission was detected between 463 and 581 nm, and mVenus emission was detected between 526 and 598 nm. The multichannel images were processed using the spectral unmixing plugin in ImageJ and then merged.⁶⁸

Image levels and brightness were applied to the whole image in Adobe Photoshop (CS6), except for those images that were used for intensity measurements.

Computational Modeling. All symmetry-breaking and domain-specific growth regulation modules were created as python scripts and run in CellModeller (<http://haselofflab.github.io/CellModeller/>). All these Python modules and MATLAB scripts used for data analysis are available at <https://github.com/timrudge/MorphoEngineering>.

■ ASSOCIATED CONTENT

📄 Supporting Information

The Supporting Information is available free of charge on the ACS Publications website at DOI: 10.1021/acssynbio.6b00149.

Extended materials and methods, as well as oligonucleotide Figures S1–S10 (PDF)

CellModeller simulations (ZIP)

■ AUTHOR INFORMATION

Corresponding Author

*E-mail: ffederici@bio.puc.cl.

Author Contributions

#I.N.N., T.F.M., and I.D.D.V. contributed equally to this work

Notes

The authors declare no competing financial interest.

■ ACKNOWLEDGMENTS

T.J.R., A.K., and J.H. were supported by the UK Biotechnological and Biological Sciences Research Council (BBSRC) Synthetic Biology Research Centre “OpenPlant” award (BB/L014130/1), F.F. was supported by CONICYT-PAI/Concurso Nacional de Apoyo al Retorno de Investigadores/as desde el Extranjero Folio 82130027, Fondo de Desarrollo de Areas Prioritarias (FONDAP) Center for Genome Regulation (15090007), Millennium Nucleus Center for Plant Systems and Synthetic Biology (NC130030) and Fondecyt Iniciación

11140776. A.K. was also supported by BBSRC CASE studentship in partnership with Microsoft Research. A.C. and D.E. were supported by NSF GRFP fellowship and Stanford University. This material is based upon work supported by the National Science Foundation Graduate Research Fellowship Program under Grant No. DGE-114747 and additional support was provided by Stanford University. The authors would like to thank Rodrigo Gutierrez and his group (PUC, Chile) for support and useful comments, Joseph Torella and Pam Silver for UNSes vectors, Cambridge 2009 iGEM team for violacein operon, Registry of Biological Parts (MIT) for RNAPT7, fluorescent proteins, and pSB4K5 vector. pdCas9 was a gift from Luciano Marraffini (Addgene plasmid # 46569).

■ REFERENCES

- (1) Benenson, Y. (2012) Biomolecular computing systems: principles, progress and potential. *Nat. Rev. Genet.* 13, 455–468.
- (2) Chen, A. Y., Deng, Z., Billings, A. N., Seker, U. O., Lu, M. Y., Citorik, R. J., Zakeri, B., and Lu, T. K. (2014) Synthesis and patterning of tunable multiscale materials with engineered cells. *Nat. Mater.* 13, 515–523.
- (3) Didovyyk, A., Kanakov, O. I., Ivanchenko, M. V., Hasty, J., Huerta, R., and Tsimring, L. (2015) Distributed classifier based on genetically engineered bacterial cell cultures. *ACS Synth. Biol.* 4, 72–82.
- (4) Douglas, S. M., Bachelet, I., and Church, G. M. (2012) A logic-gated nanorobot for targeted transport of molecular payloads. *Science* 335, 831–834.
- (5) Galanie, S., Thodey, K., Trenchard, I. J., Filsinger Interrante, M., and Smolke, C. D. (2015) Complete biosynthesis of opioids in yeast. *Science* 349, 1095–1100.
- (6) Macia, J., and Sole, R. (2014) How to make a synthetic multicellular computer. *PLoS One* 9, e81248.
- (7) Nielsen, A. A., Der, B. S., Shin, J., Vaidyanathan, P., Paralanov, V., Strychalski, E. A., and Voigt, C. A. (2016) Genetic circuit design automation. *Science* 352 (6281), aac7341.
- (8) Qian, L., Winfree, E., and Bruck, J. (2011) Neural network computation with DNA strand displacement cascades. *Nature* 475, 368–372.
- (9) Siuti, P., Yazbek, J., and Lu, T. K. (2013) Synthetic circuits integrating logic and memory in living cells. *Nat. Biotechnol.* 31, 448–452.
- (10) Xie, Z., Wroblewska, L., Prochazka, L., Weiss, R., and Benenson, Y. (2011) Multi-input RNAi-based logic circuit for identification of specific cancer cells. *Science* 333, 1307.
- (11) Ausländer, S., Ausländer, D., Müller, M., Wieland, M., and Fussenegger, M. (2012) Programmable single-cell mammalian biocomputers. *Nature* 487, 123–127.
- (12) Danino, T., Mondragón-Palomino, O., Tsimring, L., and Hasty, J. (2010) A synchronized quorum of genetic clocks. *Nature* 463, 326–330.
- (13) Del Vecchio, D. (2015) Modularity, context-dependence, and insulation in engineered biological circuits. *Trends Biotechnol.* 33, 111–119.
- (14) Kosuri, S., Goodman, D. B., Cambray, G., Mutalik, V. K., Gao, Y., Arkin, A. P., Endy, D., and Church, G. M. (2013) Composability of regulatory sequences controlling transcription and translation in *Escherichia coli*. *Proc. Natl. Acad. Sci. U. S. A.* 110, 14024–14029.
- (15) Liu, C. C., Qi, L., Lucks, J. B., Segall-Shapiro, T. H., Wang, D., Mutalik, V. K., and Arkin, A. P. (2012) An adaptor from translational to transcriptional control enables predictable assembly of complex regulation. *Nat. Methods* 9, 1088–1094.
- (16) Lou, C., Stanton, B., Chen, Y. J., Munsky, B., and Voigt, C. A. (2012) Ribozyme-based insulator parts buffer synthetic circuits from genetic context. *Nat. Biotechnol.* 30, 1137–1142.
- (17) Mutalik, V. K., Guimaraes, J. C., Cambray, G., Lam, C., Christoffersen, M. J., Mai, Q. A., Tran, A. B., Paull, M., Keasling, J. D., Arkin, A. P., and Endy, D. (2013) Precise and reliable gene expression

via standard transcription and translation initiation elements. *Nat. Methods* 10, 354–360.

(18) Qi, L., Haurwitz, R. E., Shao, W., Doudna, J. A., and Arkin, A. P. (2012) RNA processing enables predictable programming of gene expression. *Nat. Biotechnol.* 30, 1002–1006.

(19) Purnick, P. E., and Weiss, R. (2009) The second wave of synthetic biology: from modules to systems. *Nat. Rev. Mol. Cell Biol.* 10, 410–422.

(20) Balagaddé, F. K., Song, H., Ozaki, J., Collins, C. H., Barnet, M., Arnold, F. H., Quake, S. R., and You, L. (2008) A synthetic Escherichia coli predator-prey ecosystem. *Mol. Syst. Biol.* 4, 187.

(21) Basu, S., Gerchman, Y., Collins, C. H., Arnold, F. H., and Weiss, R. (2005) A synthetic multicellular system for programmed pattern formation. *Nature* 434, 1130–1134.

(22) Ji, W., Shi, H., Zhang, H., Sun, R., Xi, J., Wen, D., Feng, J., Chen, Y., Qin, X., Ma, Y., Luo, W., Deng, L., Lin, H., Yu, R., and Ouyang, Q. (2013) A formalized design process for bacterial consortia that perform logic computing. *PLoS One* 8, e57482.

(23) Liu, C., Fu, X., Liu, L., Ren, X., Chau, C. K. L., Li, S., Xiang, L., Zeng, H., Chen, G., and Tang, L. H. (2011) Sequential establishment of stripe patterns in an expanding cell population. *Science Signalling* 334, 238.

(24) Regot, S., Macia, J., Conde, N., Furukawa, K., Kjellén, J., Peeters, T., Hohmann, S., de Nadal, E., Posas, F., and Solé, R. (2011) Distributed biological computation with multicellular engineered networks. *Nature* 469, 207–211.

(25) Schaeferli, Y., Munteanu, A., Gili, M., Cotterell, J., Sharpe, J., and Isalan, M. (2014) A unified design space of synthetic stripe-forming networks. *Nat. Commun.* 5, No. 4905.

(26) Tamsir, A., Tabor, J. J., and Voigt, C. A. (2011) Robust multicellular computing using genetically encoded NOR gates and chemical/wires/. *Nature* 469, 212–215.

(27) Zhou, K., Qiao, K., Edgar, S., and Stephanopoulos, G. (2015) Distributing a metabolic pathway among a microbial consortium enhances production of natural products. *Nat. Biotechnol.* 33, 377–383.

(28) Doursat, R., Sayama, H., and Michel, O. (2013) A review of morphogenetic engineering. *Nat. Comput.* 12, 517–535.

(29) Doursat, R., Sayama, H., and Michel, O. (2012) *Morphogenetic Engineering: Toward Programmable Complex Systems*, Springer.

(30) Chen, A. Y., Zhong, C., and Lu, T. K. (2015) Engineering living functional materials. *ACS Synth. Biol.* 4, 8–11.

(31) Ball, P., and Borley, N. R. (1999) *The self-made tapestry: pattern formation in nature*, Oxford University Press, Oxford.

(32) Goodwin, B. C., Kauffman, S., and Murray, J. D. (1993) Is morphogenesis an intrinsically robust process? *J. Theor. Biol.* 163, 135–144.

(33) Bashor, C. J., Horwitz, A. A., Peisajovich, S. G., and Lim, W. A. (2010) Rewiring cells: synthetic biology as a tool to interrogate the organizational principles of living systems. *Annu. Rev. Biophys.* 39, 515.

(34) Holland, J. H. (2012) *Signals and boundaries: Building blocks for complex adaptive systems*, MIT Press.

(35) Grant, P. K., Dalchau, N., Brown, J. R., Federici, F., Rudge, T. J., Yordanov, B., Patange, O., Phillips, A., and Haseloff, J. (2016) Orthogonal intercellular signaling for programmed spatial behavior. *Mol. Syst. Biol.* 12, 849.

(36) Payne, S., Li, B., Cao, Y., Schaeffer, D., Ryser, M. D., and You, L. (2013) Temporal control of self-organized pattern formation without morphogen gradients in bacteria. *Mol. Syst. Biol.* 9, 697.

(37) Cachat, E., Liu, W., Hohenstein, P., and Davies, J. A. (2014) A library of mammalian effector modules for synthetic morphology. *J. Biol. Eng.* 8, 1.

(38) Pascalie, J., Potier, M., Kowaliw, T., Giavitto, J.-L., Michel, O., Spicher, A., and Doursat, R. (2016) Developmental design of synthetic bacterial architectures by morphogenetic engineering. *ACS Synth. Biol.* 5, 842–61.

(39) Davies, J. A. (2008) Synthetic morphology: prospects for engineered, self-constructing anatomies. *J. Anat.* 212, 707–719.

(40) Foty, R. A., and Steinberg, M. S. (2005) The differential adhesion hypothesis: a direct evaluation. *Dev. Biol.* 278, 255–263.

(41) Bowman, J. L., Smyth, D. R., and Meyerowitz, E. M. (2012) The ABC model of flower development: then and now. *Development* 139, 4095–4098.

(42) Rudge, T. J., Steiner, P. J., Phillips, A., and Haseloff, J. (2012) Computational modeling of synthetic microbial biofilms. *ACS Synth. Biol.* 1, 345–352.

(43) Rudge, T. J., Federici, F., Steiner, P. J., Kan, A., and Haseloff, J. (2013) Cell Polarity-Driven Instability Generates Self-Organized, Fractal Patterning of Cell Layers. *ACS Synth. Biol.* 2, 705–714.

(44) Anderson, P. W. (1972) More is different. *Science* 177, 393–396.

(45) Gierer, A., and Meinhardt, H. (1972) A theory of biological pattern formation. *Biological Cybernetics* 12, 30–39.

(46) Munro, E., and Bowerman, B. (2009) Cellular symmetry breaking during Caenorhabditis elegans development. *Cold Spring Harbor Perspect. Biol.* 1, a003400.

(47) Tompkins, N., Li, N., Girabawe, C., Heymann, M., Ermentrout, G. B., Epstein, I. R., and Fraden, S. (2014) Testing Turing's theory of morphogenesis in chemical cells. *Proc. Natl. Acad. Sci. U. S. A.* 111, 4397–4402.

(48) Turing, A. M. (1952) The chemical basis of morphogenesis. *Philos. Trans. R. Soc., B* 237, 37–72.

(49) van der Gucht, J., and Sykes, C. (2009) Physical model of cellular symmetry breaking. *Cold Spring Harbor Perspect. Biol.* 1, a001909.

(50) Wennekamp, S., Mesecke, S., Nédélec, F., and Hiiragi, T. (2013) A self-organization framework for symmetry breaking in the mammalian embryo. *Nat. Rev. Mol. Cell Biol.* 14, 452–459.

(51) Torella, J. P., Boehm, C. R., Lienert, F., Chen, J. H., Way, J. C., and Silver, P. A. (2014) Rapid construction of insulated genetic circuits via synthetic sequence-guided isothermal assembly. *Nucleic Acids Res.* 42, 681–689.

(52) Chen, Y. J., Liu, P., Nielsen, A. A., Brophy, J. A., Clancy, K., Peterson, T., and Voigt, C. A. (2013) Characterization of 582 natural and synthetic terminators and quantification of their design constraints. *Nat. Methods* 10, 659–664.

(53) Dahmann, C., Oates, A. C., and Brand, M. (2011) Boundary formation and maintenance in tissue development. *Nat. Rev. Genet.* 12, 43–55.

(54) August, P. R., Grossman, T. H., Minor, C., Draper, M. P., MacNeil, I. A., Pemberton, J. M., Call, K. M., Holt, D., and Osburne, M. S. (2000) Sequence analysis and functional characterization of the violacein biosynthetic pathway from Chromobacterium violaceum. *J. Mol. Microbiol. Biotechnol.* 2, 513–519.

(55) Segall-Shapiro, T. H., Meyer, A. J., Ellington, A. D., Sontag, E. D., and Voigt, C. A. (2014) A 'resource allocator' for transcription based on a highly fragmented T7 RNA polymerase. *Mol. Syst. Biol.* 10, 742.

(56) Newman, S. A., and Bhat, R. (2009) Dynamical patterning modules: a "pattern language" for development and evolution of multicellular form. *Int. J. Dev. Biol.* 53, 693–705.

(57) Noorduyn, W. L., Grinthal, A., Mahadevan, L., and Aizenberg, J. (2013) Rationally designed complex, hierarchical microarchitectures. *Science* 340, 832–837.

(58) Werfel, J., Petersen, K., and Nagpal, R. (2014) Designing collective behavior in a termite-inspired robot construction team. *Science* 343, 754–758.

(59) Isalan, M., Lemerle, C., and Serrano, L. (2005) Engineering gene networks to emulate Drosophila embryonic pattern formation. *PLoS Biol.* 3, e64.

(60) Korolev, K. S., Müller, M. J., Karahan, N., Murray, A. W., Hallatschek, O., and Nelson, D. R. (2012) Selective sweeps in growing microbial colonies. *Phys. Biol.* 9, 026008.

(61) Blanchard, A. E., and Lu, T. (2015) Bacterial social interactions drive the emergence of differential spatial colony structures. *BMC Syst. Biol.* 9, 59.

- (62) Brenner, K., and Arnold, F. H. (2011) Self-organization, layered structure, and aggregation enhance persistence of a synthetic biofilm consortium. *PLoS One* 6, e16791.
- (63) Hallatschek, O., Hersen, P., Ramanathan, S., and Nelson, D. R. (2007) Genetic drift at expanding frontiers promotes gene segregation. *Proc. Natl. Acad. Sci. U. S. A.* 104, 19926–19930.
- (64) Hauert, C., and Doebeli, M. (2004) Spatial structure often inhibits the evolution of cooperation in the snowdrift game. *Nat. Mater.* 428, 643–646.
- (65) Kovács, T. (2014) Impact of spatial distribution on the development of mutualism in microbes. *Front Microbiol.* 5, 649.
- (66) Hol, F. J., Galajda, P., Woolthuis, R. G., Dekker, C., and Keymer, J. E. (2015) The idiosyncrasy of spatial structure in bacterial competition. *BMC Res. Notes* 8, 245.
- (67) Gibson, D. G., Young, L., Chuang, R. Y., Venter, J. C., Hutchison, C. A., and Smith, H. O. (2009) Enzymatic assembly of DNA molecules up to several hundred kilobases. *Nat. Methods* 6, 343–345.
- (68) Schneider, C. A., Rasband, W. S., and Eliceiri, K. W. (2012) NIH Image to ImageJ: 25 years of image analysis. *Nat. Methods* 9, 671–675.